Collision

YU-CHIA LIN*
Department of Physics & Astronomy, University of New Mexicoo, Albuquerque, New Mexico 87131, USA
Department of Astronomy, University of Arizona, Tucson, Arizona 85721, USA and
Department of Physics, University of Arizona, Tucson, Arizona 85721, USA
(Dated: September 29, 2022)

It has been a long-standing mystery how collisions and collective neutrino oscillations interact. We focus on one type of collision-generated instabilities as we investigate the impact of the collision term in neutrino flavor oscillations. In this model, the instability that may be common inside supernovae is caused by an asymmetry in the collisional interactions between neutrinos and antineutrinos. By creating analytical solutions, we sought to gain insight into such a mechanism.

Additionally, our analytical approach demonstrates precisely when the exponential growth brought on by this instability begins, how quickly it increases, and how different factors affect the bump, making it potentially meaningful to a wider variety of collision-generated instabilities models.

I. INTRODUCTION

A.

1.

II. MODEL

In this work, we consider the isotropic and homogeneous two-flavor neutrino flavor oscillation between ν_e and ν_τ, where ν_τ represents a linear combination of the physical μ and τ flavor neutrino.

Denoting the neutrino flavor density matrix and the corresponding polarization vector as

$$\rho = \begin{bmatrix} \rho_{11} & \rho_{12} \\ \rho_{21} & \rho_{22} \end{bmatrix} \tag{1}$$

and $\mathbf{P}$ respectively, or

$$\rho_{ex} \equiv \rho_{21} = \frac{1}{2}\left(P_x + iP_y\right) \tag{2}$$

$$\rho = \frac{1}{2}\left(P_0 + \mathbf{P}\cdot\sigma\right) \tag{3}$$

, where P_i is the i component of $\mathbf{P}$.

As for the collision processes(P), we consider three types processes, absorption and emission (AE), charged current scattering (CC), and neutral-current scattering (NC). The corresponding polarization vectors in equilibrium states and are denoted as $\mathbf{P}^P$ and P_0^P. Also, the corresponding coefficients for each process are $\Gamma_P = diag\left(\Gamma_e^P/2,\ \Gamma_x^P/2\right)$, and we could define $\Gamma_\pm^P = \left(\Gamma_e^P \pm \Gamma_x^P\right)/2$.

There are the same parameters for antineutrinos, and the bar cap is added to indicate. Then, we could write down the equations of motion for polarization vectors as follows (see Ref. [1]):

$$\dot{\mathbf{P}} = \omega\mathbf{B}\times\mathbf{P} + \mu(\mathbf{P}-\bar{\mathbf{P}})\times\mathbf{P} - \Gamma_+^{CC}\mathbf{P}_T + \Gamma_+^{AE}(\mathbf{P}^{AE}-\mathbf{P}) + \Gamma_-^{AE}(P_0^{AE}-P_0)\mathbf{z} \tag{4}$$

$$\dot{\bar{\mathbf{P}}} = -\omega\mathbf{B}\times\bar{\mathbf{P}} + \mu(\mathbf{P}-\bar{\mathbf{P}})\times\bar{\mathbf{P}} - \bar{\Gamma}_+^{CC}\bar{\mathbf{P}}_T + \bar{\Gamma}_+^{AE}(\bar{\mathbf{P}}^{AE}-\bar{\mathbf{P}}) + \bar{\Gamma}_-^{AE}(\bar{P}_0^{AE}-\bar{P}_0)\mathbf{z} \tag{5}$$

$$\dot{P}_0 = \Gamma_+^{AE}(P_0^{AE}-P_0) + \Gamma_-^{AE}(P_z^{AE}-P_z) \tag{6}$$

$$\dot{\bar{P}}_0 = \bar{\Gamma}_+^{AE}(\bar{P}_0^{AE}-\bar{P}_0) + \bar{\Gamma}_-^{AE}(\bar{P}_z^{AE}-\bar{P}_z) \tag{7}$$

, where angular frequency in vacuum $\omega = \frac{\delta m^2}{2E}$ and $\mu = \sqrt{2}G_F$.

In the following calculations, unless otherwise specified, we choose the following parameter values

$$\begin{bmatrix} \omega \\ \mu \\ \theta \\ \mathbf{B} \end{bmatrix} = \begin{bmatrix} 0.3\ km^{-1} \\ 6\times10^5\ km^{-1} \\ 10^{-6} \\ -sin2\theta\ \mathbf{e}_x^f + cos2\theta\ \mathbf{e}_z^f \end{bmatrix} \tag{8}$$

$$\begin{bmatrix} \Gamma_+^{CC} \\ \Gamma_+^{AE} \\ \Gamma_-^{AE} \end{bmatrix} = \begin{bmatrix} 0.5/11.4\ km^{-1} \\ 0.5/0.417\ km^{-1} \\ 0.5/0.417\ km^{-1} \end{bmatrix} \tag{9}$$

* yuchialin@arizona.edu

$$\begin{bmatrix} \bar{\Gamma}^{CC} \\ \bar{\Gamma}^{AE}_{+} \\ \bar{\Gamma}^{AE}_{-} \end{bmatrix} = \begin{bmatrix} 0.5/37.2\ km^{-1} \\ 0.5/4.36\ km^{-1} \\ 0.5/4.36\ km^{-1} \end{bmatrix} \tag{10}$$

$$\begin{bmatrix} \mathbf{P}^{AE} \\ P_0^{AE} \\ \bar{\mathbf{P}}^{AE} \\ \bar{P}_0^{AE} \end{bmatrix} = \begin{bmatrix} 2\ \mathbf{e}_z^f \\ 4 \\ 1.5\ \mathbf{e}_z^f \\ 3.5 \end{bmatrix} \tag{11}$$

Also, the initial condition

$$\begin{bmatrix} \mathbf{P} \\ P_0 \\ \bar{\mathbf{P}} \\ \bar{P}_0 \end{bmatrix} = \begin{bmatrix} 2\ \mathbf{e}_z^f \\ 4 \\ 1.5\ \mathbf{e}_z^f \\ 3.5 \end{bmatrix} \tag{12}$$

Note that we use $10^{33}\ cm^{-3}$ as the unit length in the vector space of polarization vectors.

III. RESULTS

Here we will try to solve the equations of motion in the linear region and compare the analytical results with the numerical results. With this analytical solution, we could find an approximate expression for the start time and the growth rate of exponential growth in the limit cases, which characterize the bump.

A. Numerical Solution

Given initial conditions and parameters as described in equation (8), (9), (10), (11), and (12), we could obtain the numerical solutions via the equations of motion of polarization vectors. We plot the results in FIG. 1 and show them as solid lines.

It should be emphasized that there is a requirement for the precision of numerical simulations in order to produce consistent results. We need to be quite careful, especially when μ are really large or θ is quite little. The detailed reasoning behind it will be discussed in subsection IV A.

B. Linearlized Equations of Motion

We need to determine when the equations of motion is a system of linear equations in order to obtain an analytical solution. Actually, when $P_x,\ P_y \ll P_z \sim 1$, the equations of motion become

$$i\partial_t \rho_{ex} = \omega\ sin2\theta P_z + \left[-\omega\ cos2\theta - \sqrt{2}G_F(n_{\bar{\nu}_e} - n_{\bar{\nu}_x}) - i\Gamma\right]\rho_{ex} + \sqrt{2}G_F(n_{\nu_e} - n_{\nu_x})\bar{\rho}_{ex} \tag{13}$$

$$i\partial_t \bar{\rho}_{ex} = -\omega\ sin2\theta \bar{P}_z + \left[+\omega\ cos2\theta + \sqrt{2}G_F(n_{\nu_e} - n_{\nu_x}) - i\bar{\Gamma}\right]\bar{\rho}_{ex} - \sqrt{2}G_F(n_{\bar{\nu}_e} - n_{\bar{\nu}_x})\rho_{ex} \tag{14}$$

, where

$$\begin{cases} \Gamma \equiv \Gamma^{AE} + \Gamma^{CC} \\ \bar{\Gamma} \equiv \bar{\Gamma}^{AE} + \bar{\Gamma}^{CC} \end{cases} \tag{15}$$

Let

$$\begin{cases} \mu_+ \equiv \left(\frac{S+D}{2}\right)\mu \\ \mu_- \equiv \left(\frac{S-D}{2}\right)\mu \end{cases} \tag{16}$$

,

$$\begin{cases} S \equiv |\vec{S}(0)| = n_{\nu_e} - n_{\nu_x} + n_{\bar{\nu}_e} - n_{\bar{\nu}_x} \\ D \equiv |\vec{D}(0)| = n_{\nu_e} - n_{\nu_x} - n_{\bar{\nu}_e} + n_{\bar{\nu}_x} \end{cases} \tag{17}$$

, and

$$A = \begin{bmatrix} -\omega\ cos2\theta - \mu_- - i\Gamma & \mu_+ \\ -\mu_- & \omega\ cos2\theta + \mu_+ - i\bar{\Gamma} \end{bmatrix} \tag{18}$$

, we have

$$i\partial_t \begin{bmatrix} \rho_{ex} \\ \bar{\rho}_{ex} \end{bmatrix} = \begin{bmatrix} \omega\ sin2\theta \\ -\omega\ sin2\theta \end{bmatrix} + A \begin{bmatrix} \rho_{ex} \\ \bar{\rho}_{ex} \end{bmatrix} \tag{19}$$

Notice that, P_z and $\bar{P}_z$ are both close to 1 under this limitation condition.

C. Analytic Solution

Assume

$$\begin{cases} \rho_{ex}(t) = \rho_{ex}^0 + Qe^{-i\Omega t} \\ \bar{\rho}_{ex}(t) = \bar{\rho}_{ex}^0 + \bar{Q}e^{-i\Omega t} \end{cases} \tag{20}$$

from equation (19), we then have

$$\Omega \begin{bmatrix} Q \\ \bar{Q} \end{bmatrix} = A \begin{bmatrix} Q \\ \bar{Q} \end{bmatrix} \tag{21}$$

, where ρ_{ex}^0 and $\bar{\rho}_{ex}^0$ satisfy

$$0 = \begin{bmatrix} \omega\ sin2\theta \\ -\omega\ sin2\theta \end{bmatrix} + A \begin{bmatrix} \rho_{ex}^0 \\ \bar{\rho}_{ex}^0 \end{bmatrix} \tag{22}$$

Therefore, we could solve the eigenvalue problem of matrix A, and denote the eigenvalues and normalized eigenvectors as $\Omega_\pm$ and $\vec{v}_\pm$ respectively.

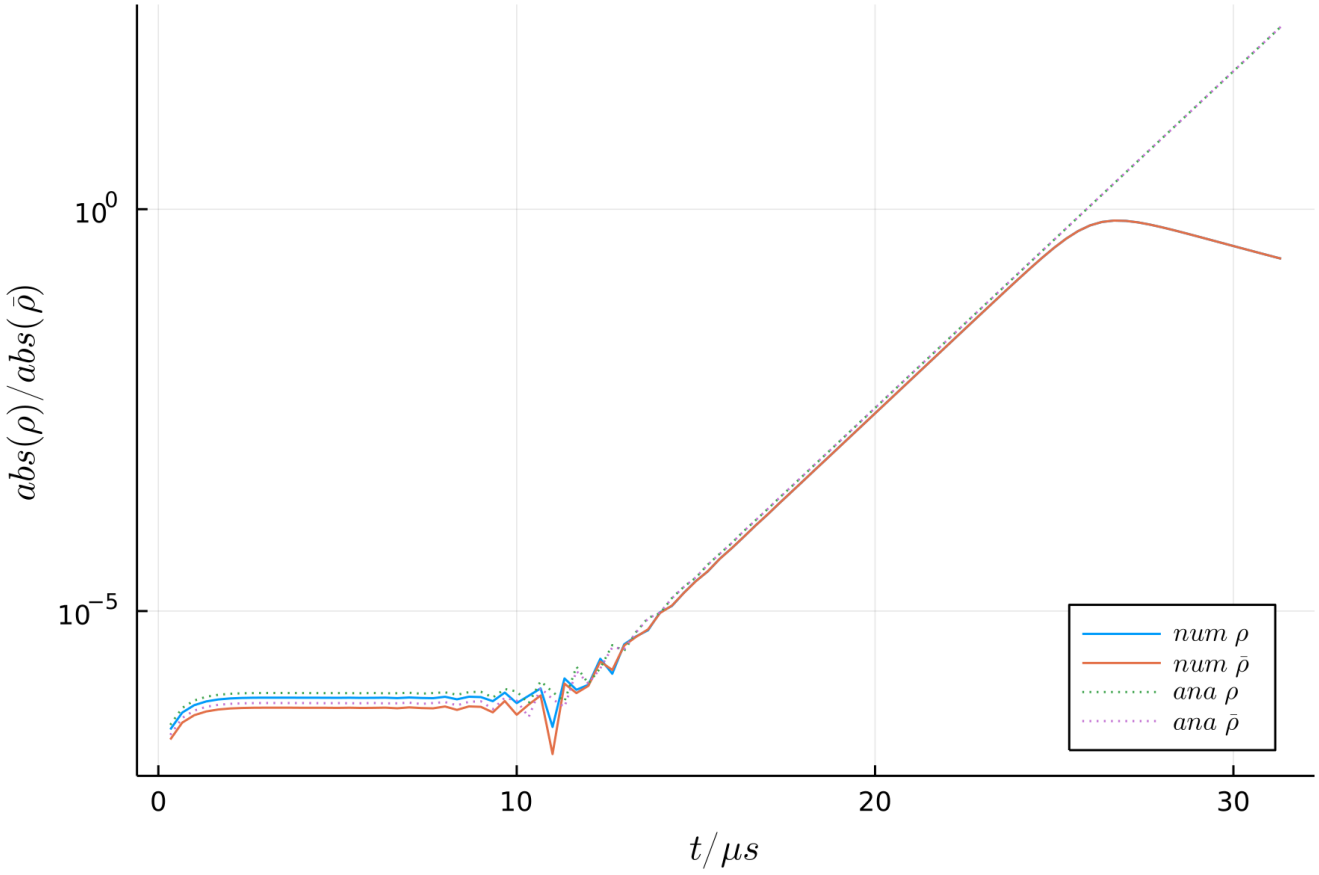

FIG. 1. The absolute value of ρ_{ex} and $\bar{\rho}_{ex}$ over time

Then,

$$\begin{aligned}\begin{bmatrix}\rho_{ex}(t)\\ \bar{\rho}_{ex}(t)\end{bmatrix} &= \begin{bmatrix}\rho^0_{ex}\\ \bar{\rho}^0_{ex}\end{bmatrix} + Q_+\vec{v}_+ e^{-i\Omega_+\mathbf{t}} + Q_-\vec{v}_- e^{-i\Omega_-\mathbf{t}} \\ &= v\begin{bmatrix}Q_- e^{-i\Omega_-\mathbf{t}}\\ Q_+ e^{-i\Omega_+\ \mathbf{t}}\end{bmatrix} + \begin{bmatrix}\rho^0_{ex}\\ \bar{\rho}^0_{ex}\end{bmatrix} \end{aligned} \tag{23}$$

, where

$$v \equiv \begin{bmatrix}\vec{v}_- & \vec{v}_+\end{bmatrix} \tag{24}$$

and Q_+ and Q_- satisfy

$$\begin{bmatrix}Q_-\\ Q_+\end{bmatrix} = v^{-1}\begin{bmatrix}-\rho^0_{ex}\\ -\bar{\rho}^0_{ex}\end{bmatrix} \tag{25}$$

Now, we could compare this analytical solution with the numerical solution in FIG. 1.

D. Approximate and Analytical Expressions

In this subsection, we consider $\mu S,\ \mu D \gg \omega,\ \Gamma,\ \bar{\Gamma}$ and $\theta \ll 1$. Then, the zero order approximation of equation

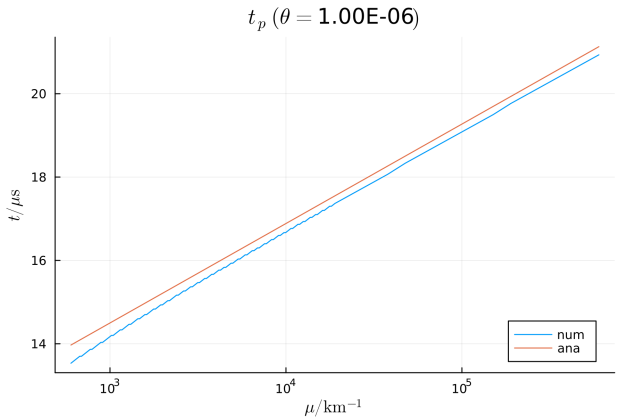

FIG. 2. Comparing t_p in equation (37) with numerical simulation for different μ

(22)

$$\begin{bmatrix}\rho^0_{ex}\\ \bar{\rho}^0_{ex}\end{bmatrix} = A^{-1}\begin{bmatrix}-\omega\ sin2\theta\\ +\omega\ sin2\theta\end{bmatrix} \simeq \frac{2\omega\theta}{\omega S + i\left[(S+D)\Gamma + (D-S)\bar{\Gamma}\right]}\begin{bmatrix}S+D\\ S-D\end{bmatrix} \quad (26)$$

$$\sim \theta^1\mu^0 \quad (27)$$

On the other hand, the eigenvalues of A is

$$\begin{bmatrix}\Omega_+\\ \Omega_-\end{bmatrix} \simeq \begin{bmatrix}\mu D + i\left[\frac{S}{2D}\left(\Gamma-\bar{\Gamma}\right) - \frac{1}{2}\left(\Gamma+\bar{\Gamma}\right)\right]\\ \frac{\omega S}{D} - i\left[\frac{S}{2D}\left(\Gamma-\bar{\Gamma}\right) + \frac{1}{2}\left(\Gamma+\bar{\Gamma}\right)\right]\end{bmatrix} \quad (28)$$

Then, we could get the zero order approximation of the eigenvectors matrix

$$v \simeq \begin{bmatrix}\frac{S+D}{\sqrt{2}\sqrt{S^2+D^2}} & \frac{1}{\sqrt{2}}\\ \frac{S-D}{\sqrt{2}\sqrt{S^2+D^2}} & \frac{1}{\sqrt{2}}\end{bmatrix} \quad (29)$$

, or

$$v^{-1} \simeq \begin{bmatrix}\frac{\sqrt{S^2+D^2}}{\sqrt{2}D} & -\frac{\sqrt{S^2+D^2}}{\sqrt{2}D}\\ \frac{D-S}{\sqrt{2}D} & \frac{D+S}{\sqrt{2}D}\end{bmatrix} \quad (30)$$

Substituting equation (26) and equation (30) into equation (25), the zero order approximation of Q:

$$\begin{bmatrix}Q_-\\ Q_+\end{bmatrix} \simeq \frac{-4\sqrt{2}\omega\theta\sqrt{S^2+D^2}}{\omega S + i\left[(S+D)\Gamma + (D-S)\bar{\Gamma}\right]}\begin{bmatrix}1\\ 0\end{bmatrix} \quad (31)$$

Here we discover that the zeroth order of Q_+ is approximately zero, explaining why the exponential growth takes some time to start, why a high level of precision is necessary for the numerical solution to produce an accurate bump (see subsection IV A).

When $|\mathrm{Im}\{\Omega_-\}|\mathrm{t} >> 1$, equation (23) could be simplified to

$$\begin{bmatrix}\rho_{ex}(t)\\ \bar{\rho}_{ex}(t)\end{bmatrix} \simeq Q_+ e^{-i\Omega_+\ \mathbf{t}}\begin{bmatrix}v_{12}\\ v_{22}\end{bmatrix} + \begin{bmatrix}\rho^0_{ex}\\ \bar{\rho}^0_{ex}\end{bmatrix} \quad (32)$$

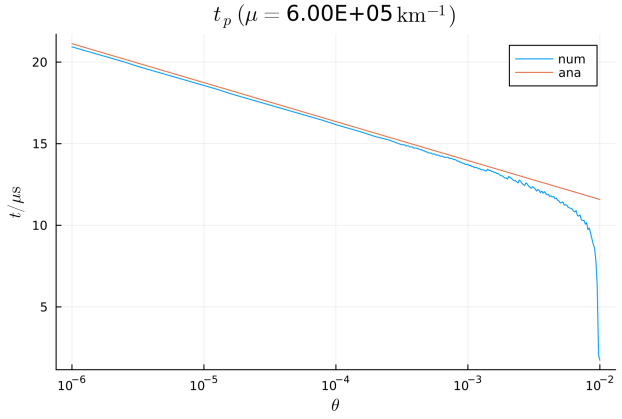

FIG. 3. Comparing t_p in equation (37) with numerical simulation for different θ

Therefore, to get the start time of the exponential growing, we have to find the first order nonzero approximation of Q_+:

$$Q_+ \simeq \frac{-2\sqrt{2}\omega\theta}{\mu\omega S - i\left[\mu_+\Gamma - \mu_-\bar{\Gamma}\right]}\begin{bmatrix}-\frac{\mu'_-}{\mu D}\\ \frac{\mu_+}{\mu D}\end{bmatrix}^T\begin{bmatrix}2\mu_+ + \omega - i\bar{\Gamma}\\ 2\mu_- + \omega + i\Gamma\end{bmatrix} \simeq \frac{-2\theta\omega S}{\mu D^2} \quad (33)$$

$$\sim \theta^1\mu^{-1} \quad (34)$$

, where $\mu'_- \equiv \mu_- + \omega + i\Gamma + \Omega_-$.

Finally, we could obtain the start time of the exponential growth

$$t_s \simeq \frac{1}{\mathrm{Im}\{\Omega_+\}} ln\left(\frac{\left|\left(\rho^0_{ex},\ \bar{\rho}^0_{ex}\right)\right|}{\left|Q_+\left(v_{12},\ v_{22}\right)\right|}\right) \simeq \frac{1}{\left[\frac{S}{2D}\left(\Gamma-\bar{\Gamma}\right) - \frac{1}{2}\left(\Gamma+\bar{\Gamma}\right)\right]} \ln\left(\frac{2\mu D^2\sqrt{S^2+D^2}}{S\sqrt{\omega^2S^2 + \left[(S+D)\Gamma + (D-S)\bar{\Gamma}\right]^2}}\right) \quad (35)$$

$$\sim \ln(\mu^1\theta^0) \quad (36)$$

which is independent of θ.

Moreover, with a similar analysis, we could get the time it takes for the absolute density, $\left|\left(\rho^0_{ex},\ \bar{\rho}^0_{ex}\right)\right|$, to reach a particular density $(\rho_p) \ll 1$:

$$t_p \simeq \frac{1}{\mathrm{Im}\{\Omega_+\}} ln\left(\frac{\rho_p}{\left|Q_+\left(v_{12},\ v_{22}\right)\right|}\right) \simeq \frac{1}{\left[\frac{S}{2D}\left(\Gamma-\bar{\Gamma}\right) - \frac{1}{2}\left(\Gamma+\bar{\Gamma}\right)\right]} \ln\left(\frac{\rho_p\mu D^2}{2\theta\omega S}\right) \quad (37)$$

$$\sim \ln(\mu^1\theta^{-1}) \quad (38)$$

For $\rho_p = 0.01$, we could compare the results of equation (37) with the numerical simulation in FIG. 2 and 3.

IV. DISCUSSION

In this section, we'll go into more detail about how analytical solutions give us detailed knowledge that will enable us to comprehend the complete model and the mechanism underlying collision-generated instabilities.

A. Precision Requirements for Numerical Simulations

Substituting the parameters into equation (33), we have

$$|Q_+| \simeq \frac{2\theta\omega S}{\mu D^2} \simeq 1.4\times10^{-11}\left(\frac{\theta}{10^{-6}}\right)\left(\frac{\mu}{6\times10^5\ \mathrm{km}^{-1}}\right)^{-1} \quad (39)$$

Therefore, to get a realistic and accurate bump shape, the numerical simulation precision should be much smaller than Q_+.

B. Deviation between Analytical Solution and Numerical Simulation

The deviation of the analytical solution derived from the linear system of equations and the numerical simulation steadily grows, as seen in FIG. 2 and 3, as θ increases or μ decreases. This is because of the influence of nonlinear terms on numerical simulations.

V. CONCLUSIONS

[1] L. Johns, Collisional flavor instabilities of supernova neutrinos, arXiv e-prints , arXiv:2104.11369 (2021), arXiv:2104.11369 [hep-ph].